

Color Superconductivity in Schwinger-Dyson Approach

– *Strange Quark Mass and Color-Flavor Unlocking Line* –

Hiroaki ABUKI^{(a,b)*}

(a) *Yukawa Institute for Theoretical Physics, Kyoto 606-8502, JAPAN*

(b) *Department of Physics, University of Tokyo, Tokyo 113-0033, JAPAN*

Abstract

Phase structure and phase transitions in dense QCD are studied using the Schwinger-Dyson (SD) method in the improved ladder approximation. We construct the Cornwall-Jackiw-Tomboulis (CJT) effective potentials at finite temperature for two types of pairing ansatz, namely the Color-Flavor locking (CFL) state and the two flavor superconducting (2SC) state. Strong coupling effects at low densities, such as the off-Fermi surface and antiquarks contribution to the pairing gap due to the large effective coupling, make the gap, critical temperature and those ratio deviate from those weak coupling values. Nevertheless, the ratio of the physical quantity for the CFL and that for the 2SC does not differ so much from the weak coupling value, as long as the pairing interaction is taken to be the same for the both cases. As a consequence, the CFL state always dominates over the 2SC state and the critical temperatures to the quark-gluon plasma (QGP) phase from both states coincides in the chiral limit. The energy gain in the CFL state relative to the 2SC state gets smaller towards the critical line dividing (μ, T) plane into the QGP and CFL phases, and thus small perturbations can remove the degeneracy of these critical lines. As one of such perturbations, the effect of the strange quark mass m_s on the quark-pairing is examined. In particular, using a simple kinematical criterion, we discuss the behaviour of the “*color-flavor unlocking line*” on which the CFL phase turns into the 2SC phase, against the variation of m_s .

*) abuki@yukawa.kyoto-u.ac.jp

§1. Introduction

It is believed that the QCD ground state changes against the variation of the external conditions, such as the baryon density, the isospin density and the strange quark mass. In particular, the color superconducting phases at high baryon density have attracted much interest in high density QCD. The asymptotic freedom of the QCD^{1),2)} leads to the smaller effective coupling at higher densities : This gives us the conjecture of deconfined quark matter³⁾ in which quarks and gluons constitute the active degrees of freedom and are weakly perturbed by the small effective coupling. Such weakly perturbed deconfined matter might be realized in the core of the neutron stars, or in possible quark stars. However, if the temperature of such deconfined system is low enough, the residual attractive force between the quarks in the color anti-triplet channel, which is supplied by either one gluon exchange (OGE) or the instanton induced interaction, leads to the instability of the Fermi surface. This instability causes the non-perturbative generation of the dynamical Majorana mass gap near the Fermi surface, which is called “color superconductivity”. Along this line, Bailin and Love made an extensive analysis on possible color superconductivities in the quark matter.⁴⁾

In recent years, there has been great developments in our understanding of the pairing phenomenology at high density. The discovery of “*Color-Flavor Locking*” (CFL) state⁵⁾ at extremely high density is one of the examples. CFL state have two types of gap in the chiral limit, namely, Δ_1 for the color-flavor singlet excitation, and Δ_8 for the octet excitations. On the other hand, the 2-flavor superconducting (2SC) state have only one gap Δ , and 4 quarks out of 9 obtain this gap. Rich physics contained in the CFL phase, as well as in the 2-flavor color superconductivity (2SC) phase, has been revealed^{6),7)}.

In our present understanding of the high density QCD, pairing patterns other than the CFL would hardly take place at high density limit^{8),9)}. It is thought that only in the presence of the finite strange quark mass $m_s \gg m_{u,d}$, the 2SC pairing appears in the low density region in the phase diagram. The color-flavor unlocking phase transition from the CFL state to the 2SC state at zero temperature have been studied using the Nambu-Jona-Lasinio (NJL) type model^{10),11)}. This transition occurs when the strange quark mass m_s at some fixed chemical potential μ gets larger than the critical mass $m_s^c(\mu)$, or equivalently when the chemical potential at some fixed m_s gets smaller than at some critical chemical potential $\mu_c(m_s)$. Analyses in Refs^{10),11)} indicate that a simple kinematical unlocking criterion $m_s^c/4\mu_c \sim |\Delta_8(\mu_c)|_{m_s=0}$ is quite a good guide for the unlocking mass and chemical potential. This criterion is based on the observation that the unlocking transition would occur at the point where the Fermi momentum for strange quark differs from those for light flavors by the smallest gap $|\Delta_8|$ for the unperturbed ($m_s = 0$) CFL state. In Ref.¹²⁾, the unlocking

(locking) transition at finite temperature is analysed in the NJL model.

In the chiral limit, weak coupling analyses of the gap equations reveal the CFL dominance over the 2SC at zero temperature and the coincidence of critical temperatures to the QGP phase from the 2SC state and from the CFL state. The former is attributed to the subtle competition^{*)} between the number of degrees of freedom participating in pairing correlation, and the magnitude of the gaps¹³⁾. The latter is due to two facts : One is the rapid vanishing of the pairing in the color sextet channel towards the critical temperature T_c . The other is the disappearance of the nonlinearity of the gap equation in the diquark condensate near T_c , and which is guaranteed if the transition is of second order. However, in the low, and physically interesting density regime, various strong coupling effects such as the participation of off-Fermi surface degrees of freedom in the formation of the gap due to the large effective coupling constant¹⁴⁾. Also the pairing in the color symmetric channel may get relevant towards low densities, although it is suppressed by one coupling constant relative to the anti-triplet one in the weak coupling regime¹³⁾. These strong coupling effects might cause a significant modification of these pictures of the CFL dominance at zero temperature and of the phase transitions. In addition, critical temperatures to the quark-gluon plasma (QGP) phase from the CFL and from the 2SC start to deviate towards low densities, although these quantities are shown to be the same in the weak coupling limit¹⁵⁾. If this is the case, the 2SC phase may show up at high temperature region.^{**)}

For the reasons mentioned above, even in the chiral limit, it would be interesting to study the pairing phenomena in dense QCD using some model having strong coupling effects at low density side. For this purpose, we examine in this paper, the Schwinger-Dyson (SD) approach in the improved ladder approximation to the color superconducting phenomena.^{14), 18) – 20)} We also use the associated Cornwall-Jackiw-Tomboulis (CJT) potential to determine which phase of (QGP, 2SC, CFL) is preferred for given density and temperature (μ, T) ⁷⁾. This approach, namely the SD equation in the Landau gauge with the improved running coupling constant can make the asymptotic behaviour of the mass function at high energy consistent with that from the operator product expansion and renormalization group argument in QCD²¹⁾. At the same time, the meson properties on the chiral-broken QCD vacuum, can be reasonably understood by the analysis of pseudo scalar Bethe-Salpeter amplitudes^{21), 22)}.

^{*)} The condensation energy in the CFL phase is about twice of that in the 2SC phase. If the ratios of the 2SC gap and the CFL gaps, $\Delta/\Delta_{1,8}$ get larger than those weak coupling values by a factor $\sqrt{2} \cong 1.4$ due to strong coupling effects, then these two phases may get nearly degenerate with each other in the energy density.

^{**)} In He^3 liquid system, the Anderson-Morel (ABM) state¹⁶⁾ shows up in the high temperature and high pressure region due to strong coupling effects, even though the Balian-Wertharmer (BW) state¹⁷⁾ has larger condensation energy in the weak coupling analysis¹⁶⁾.

Also, this approach leads to the correct dependence of the gap on the coupling constant in the weak coupling perturbative regime. Thus, we believe the improved SD approach is reliable for a wide region of the quark chemical potential. Various strong coupling effects, say, the large coupling constant, pairing correlation far away from the Fermi surface, and that for anti-quark channel, all become relevant for realistic densities in this improved SD approach^{14), 19)}. Also, we investigate the effect of the finite strange quark mass on the pairing phenomena, using a simple criterion for the color-flavor unlocking phase transition.

This paper is organized as the following. Sec. 2 is devoted to the introduction of our model and the technical details to derive the gap equations, the CJT effective potentials and other physical quantities characterizing the CFL and 2SC states. In Sec. 3, we present our numerical results. We discuss the superconducting states at finite T and study the phase transitions to normal quark matter in details at $\mu = 1000$ MeV. Also, how the 2SC and CFL states at $T = 0$ and transition temperatures T_c are modified towards the lower density region by strong coupling effects. At the last of the section, we discuss the phase diagram from our model and its dependence on the strange quark mass m_s . In Sec. 4, the summary of this work and perspective for the future work will be given.

§2. Gap equations and CJT potentials for 2SC and CFL states

In this section, we present a general framework to derive the gap equation for the given order parameter, focusing on the 2SC and CFL phases. Also, we give various physical quantities characterizing the ground state.

2.1. Gap equations for the 2SC and CFL states

Nambu-Gor'kov propagators : Here, we introduce two component quark fields $\Psi = (q, q_c)^t$ in order to express the superconducting gap as a part of the self-energy. In this Nambu-Gor'kov base, quark propagators are introduced as

$$\begin{aligned} i\mathbf{S}(p_0, \mathbf{p}) &= i \begin{pmatrix} S_{11}(p_0, \mathbf{p}) & S_{12}(p_0, \mathbf{p}) \\ S_{21}(p_0, \mathbf{p}) & S_{22}(p_0, \mathbf{p}) \end{pmatrix} \\ &= \int d^4z e^{ip_\mu z^\mu} \begin{pmatrix} \langle Tq(z)\bar{q}(0) \rangle & \langle Tq(z)\bar{q}_c(0) \rangle \\ \langle Tq_c(z)\bar{q}(0) \rangle & \langle Tq_c(z)\bar{q}_c(0) \rangle \end{pmatrix}. \end{aligned}$$

Here, the subscript c represents the charge conjugation $q^c = C\bar{q}^t$, and $\langle T\mathcal{O} \rangle$ means the ground state expectation value of the time ordered product of the composite operator \mathcal{O} . We introduce the full self-energy matrix for the quark field in this base as

$$\mathbf{\Sigma}(p_0, \mathbf{p}) = \begin{pmatrix} \Sigma_{11}(p_0, \mathbf{p}) & \Sigma_{12}(p_0, \mathbf{p}) \\ \Sigma_{21}(p_0, \mathbf{p}) & \Sigma_{22}(p_0, \mathbf{p}) \end{pmatrix}.$$

This self-energy gets dynamically generated by the interaction among quarks and defines the asymptotic quark fields. If the interaction is invariant under charge conjugation, the relation $\Sigma_{22}(p_0, \mathbf{p}) = -C\Sigma_{11}(-p_0, -\mathbf{p})^t C$ should hold. If the interaction is hermitian so that the time evolution of the system is unitary, the other relation $\Sigma_{21}(p_0, \mathbf{p}) = \gamma_0 \Sigma_{12}(p_0, \mathbf{p})^\dagger \gamma_0$ also holds. As a result, four components in $\mathbf{S}(p)$ are not independent.

$$iS_{22}(t, \mathbf{z}) = -C(iS_{11}(-t, -\mathbf{z}))^t C, \quad S_{22}(p_0, \mathbf{p}) = -CS_{11}(-p_0, -\mathbf{p})^t C, \quad (2.1)$$

$$iS_{21}(t, \mathbf{z}) = -\gamma_0(iS_{12}(-t, -\mathbf{z}))^\dagger \gamma_0, \quad S_{21}(p_0, \mathbf{p}) = \gamma_0 S_{12}(p_0, \mathbf{p})^\dagger \gamma_0. \quad (2.2)$$

Our main purpose is to investigate the density region where the chiral symmetry is already recovered. Therefore, we assume that the diagonal elements of the self-energy, namely, Dirac mass function, the deviation of the quark wave function renormalization from 1, and the radiative correction to the chemical potential are all zero. We postulate the following forms for the off-diagonal elements^{4), 23)–26)},

$$\Sigma_{12}(p_0, \mathbf{p}) = \gamma_5(\Lambda_+(\hat{p})\hat{\Delta}_-(p_0, \mathbf{p}) + \hat{\Lambda}_-(\hat{p})\hat{\Delta}_+(p_0, \mathbf{p})), \quad (2.3)$$

$$\Sigma_{21}(p_0, \mathbf{p}) = -\gamma_5(\Lambda_-(\hat{p})\hat{\Delta}_-^\dagger(p_0, \mathbf{p}) + \Lambda_+(\hat{p})\hat{\Delta}_+^\dagger(p_0, \mathbf{p})). \quad (2.4)$$

$\Lambda_\pm(\hat{p})$ in Eqs. (2.3) and (2.4) are the projection matrices for positive and negative energy states in the massless limit : $\Lambda_\pm(\hat{p}) = (1 \pm \boldsymbol{\alpha} \cdot \hat{p})/2$, where $\boldsymbol{\alpha} \equiv \gamma_0 \boldsymbol{\gamma}$ and $\hat{p} \equiv \mathbf{p}/|\mathbf{p}|$. $\hat{\Delta}_\pm(p_0, \mathbf{p})$ are the gap functions and are still matrices in the color and flavor spaces. Eigenvalues of $\hat{\Delta}_\pm$ turn out to be gap functions in quasi-quarks (+) and quasi-antiquark (–) excitations. γ_5 in Eqs. (2.3) and (2.4) guarantees that the pairing occurs in positive parity channel. Although the OGE does not distinguish the positive and negative parity channels, the instanton induced interaction which may be relevant at low densities, prefers the pairing in the positive parity channel^{27), 28)}. The Dirac structures of Eqs. (2.3) and (2.4) are of the most general pairing form for the $J = 0^+$ with aligned chirality²³⁾.*) For the moment, we proceed without specific ansatz for the color-flavor structure. The inverse of the quark propagator can be expressed as

$$\mathbf{S}^{-1}(p_0, \mathbf{p}) = \begin{pmatrix} \not{p} + \not{\mu} & -\Sigma_{12}(p_0, \mathbf{p}) \\ -\Sigma_{21}(p_0, \mathbf{p}) & \not{p} - \not{\mu} \end{pmatrix}. \quad (2.5)$$

Here $\not{\mu} = \mu \gamma_0$ and μ is the chemical potential for net quark. By taking the inverse of this expression, we get

$$S_{11}(p_0, \mathbf{p}) = +\frac{\not{p}_+}{2p} \frac{(p_0 + E_+)}{p_0^2 - E_+^2 - \hat{\Delta}_+^2} - \frac{\not{p}_-}{2p} \frac{(p_0 - E_-)}{p_0^2 - E_-^2 - \hat{\Delta}_-^2}, \quad (2.6)$$

*) There is no Cooper instability in the mixed chirality $q_L(\mathbf{q})q_R(-\mathbf{q})$ channel²⁹⁾, thus the condensate for this channel gets suppressed by the factor m_q/μ .

$$S_{12}(p_0, \mathbf{p}) = -\gamma_5 \left(\Lambda_+(\hat{p}) \frac{\hat{\Delta}_+}{p_0^2 - E_+^2 - \hat{\Delta}_+^2} + \Lambda_-(\hat{p}) \frac{\hat{\Delta}_-}{p_0^2 - E_-^2 - \hat{\Delta}_-^2} \right), \quad (2.7)$$

where we have defined $E_\pm = p \mp \mu$ and $p = |\mathbf{p}|$, the bare dispersions for quark and anti-quark in the system with the chemical potential μ . p_\pm are defined as the forward and off-forward light cone vectors, $p_\pm = (1, \pm \hat{p})$, so that $\not{p}_\pm = \gamma_0 \mp \boldsymbol{\gamma} \cdot \hat{p}$.

Gap equation as a self-consistency condition for the self-energy : The gap equations, the self-consistency conditions for $\hat{\Delta}_\pm(p_0, p)$ up to one loop order, can be expressed as the off-diagonal sector of the following Schwinger-Dyson equation in the Nambu-Gor'kov base.

$$\boldsymbol{\Sigma}(p_0, \mathbf{p}) = ig^2 \int \frac{d^4 q}{(2\pi)^4} \boldsymbol{\Gamma}_a^\mu \mathbf{S}(q_0, \mathbf{q}) \boldsymbol{\Gamma}_b^\nu(q, p) D_{\mu\nu}^{ab}(q_0 - p_0, \mathbf{q} - \mathbf{p}). \quad (2.8)$$

For simplicity, we use the bare vertex instead of the full vertex throughout this paper.

$$\boldsymbol{\Gamma}_a^\mu \equiv \begin{pmatrix} \Gamma_a^\mu & 0 \\ 0 & \bar{\Gamma}_a^\mu \end{pmatrix} = \begin{pmatrix} t_a \gamma_\mu & 0 \\ 0 & -t_a^t \gamma_\mu \end{pmatrix}. \quad (2.9)$$

t_a is defined as $\lambda_a/2$, where $\{\lambda_a\}$ are Gell-Mann matrices. The vertex $\bar{\Gamma}_A = -t_A^t \gamma_\mu$ originates from the relation $\bar{q} \Gamma_A q = -\bar{q}_c C \Gamma_A^t C q_c$. Extra minus sign purely comes from the Fermi statistics. $D_{\mu\nu}^{ab}(q_0 - p_0, \mathbf{q} - \mathbf{p}) \equiv \delta^{ab} \mathcal{D}_{\mu\nu}(q_0 - p_0, \mathbf{q} - \mathbf{p})$ is the gluon propagator in the medium, and the detailed structure of the function $\mathcal{D}_{\mu\nu}(q_0 - p_0, \mathbf{q} - \mathbf{p})$ which we use in this paper will be specified latter.

Through the positive and negative energy projection procedures, we obtain the following gap equations,

$$\begin{aligned} \hat{\Delta}_\pm(p_0, \mathbf{p}) = ig^2 \int \frac{d^4 q}{(2\pi)^4} & \left(c_{\mu\nu}(p_\mp, q_+) \frac{t_A^t \hat{\Delta}_+(q_0, \mathbf{q}) t_A}{q_0^2 - E_+^2 - \hat{\Delta}_+^2} \right. \\ & \left. + c_{\mu\nu}(p_\mp, q_-) \frac{t_A^t \hat{\Delta}_-(q_0, \mathbf{q}) t_A}{q_0^2 - E_-^2 - \hat{\Delta}_-^2} \right) \mathcal{D}_{\mu\nu}(q_0 - p_0, \mathbf{q} - \mathbf{p}), \end{aligned} \quad (2.10)$$

where we have defined $c_{\mu\nu}(p, q)$ by $c_{\mu\nu}(p_\pm, q_\pm) \equiv -(1/2) \text{tr}(\Lambda_\pm(\hat{p}) \gamma_\mu \Lambda_\pm(\hat{q}) \gamma_\nu)$

Color-flavor structure of the gap matrix in the 2-flavor case : In the 2 flavor case, the gap matrix in the color-flavor space is specified as⁴⁾:

$$\hat{\Delta}_\pm^{2\text{SC}}(p_0, \mathbf{p}) = (\tau_2 \times \lambda_2)_{ij}^{ab} \Delta_\pm(p_0, \mathbf{p}). \quad (2.11)$$

Because $\tau_2 \lambda_2$ is rank 4 matrix in the color-flavor space, 5 quarks (gu, gd, gs, rs, bs) corresponding to five eigenvectors with zero eigenvalue of the gap matrix remain gapless. These quarks contain the quantum number *strangeness* or *green color*, which does not take part in pairing. Other 4 modes belonging to the unbroken $SU(2)_c \times SU(2)_f$ doublets [$\mathbf{2}_{(r,b)}, \mathbf{2}_{(u,d)}$]

obtain the finite gaps Δ_{\pm} . The spectral density matrix ρ for the 2SC state can be extracted from the retarded propagator S_{2SC}^R . Its off-diagonal element ρ_{12} can be written as

$$\rho_{12}^{2SC}(p_0, \mathbf{p}) = -(\tau_2 \lambda_2)_{ij}^{ab} \left[\gamma_5 \Lambda_+(\hat{p}) \Delta_+ 2\pi\epsilon(p_0) \delta(p_0^2 - E_+^2 - \Delta_+^2) - \gamma_5 \Lambda_-(\hat{p}) \Delta_- 2\pi\epsilon(p_0) \delta(p_0^2 - E_-^2 - \Delta_-^2) \right]. \quad (2.12)$$

The conditions $p_0^2 - E_{\pm}^2 - \Delta_{\pm}(p_0, \mathbf{p})^2 = 0$ define the quasi-quark and quasi-antiquark dispersions.

Color-flavor structure of the gap matrix in the 3-flavor case : The color-flavor locked state is defined as⁵⁾,

$$\hat{\Delta}_{\pm}^{CFL}(p_0, p) = (P_1)_{ij}^{ab} \Delta_{\pm}^1(p_0, p) + (\bar{P}_8)_{ij}^{ab} \Delta_{\pm}^8(p_0, p), \quad (2.13)$$

$$= \frac{1}{N_c} \delta_i^a \delta_j^b \Delta_{\pm}^1 + \left(\delta_j^a \delta_i^b - \frac{1}{N_c} \delta_i^a \delta_j^b \right) \Delta_{\pm}^8. \quad (2.14)$$

The matrix $\hat{\Delta}$ is full-ranked in the color-flavor space, which results in generating gaps in all quasi-quark excitations.*) In the chiral limit, the CFL state has two-types of gap, corresponding to two eigenvalues in this matrix, one being Δ_1 and the other being Δ_8 . $P_{1(8)}$ is the projection to the asymptotic quark which transforms as singlet (octet) under the simultaneous inverse rotation $SU(3)_{C+V} \in SU(3)_c \times SU(3)_f$ in the color-flavor mixed space.**)

The CFL order parameter (2.13) can be divided into states in the color multiplets ($\bar{\mathbf{3}}_c, \mathbf{6}_c$) as

$$\hat{\Delta}^{CFL} = \epsilon^{Iab} \epsilon_{Iij} \Delta_A + (\delta_i^a \delta_j^b + \delta_j^a \delta_i^b) \Delta_S \quad (2.15)$$

$$\Delta_A = \frac{1}{6} \Delta^1 - \frac{2}{3} \Delta^8, \quad \Delta_S = \frac{1}{6} \Delta^1 + \frac{1}{3} \Delta^8, \quad (2.16)$$

where $N_c = 3$ is taken. Δ_A represents self-energy in the color anti-symmetric and flavor antisymmetric channel, where the attraction works. However, it turns out that the nonzero Δ_S gets induced in a non-perturbative way as a result of the self-consistent treatment of the gap equation⁵⁾. One can easily extract the spectral density for off-diagonal propagator,

$$\rho_{12}^{CFL}(p_0, \mathbf{p}) = -(P_1)_{ij}^{ab} \left[\gamma_5 \Lambda_+ \Delta_{1+} 2\pi\epsilon(p_0) \delta(p_0^2 - E_+^2 - \Delta_{1+}^2) + \gamma_5 \Lambda_- \Delta_{1-} 2\pi\epsilon(p_0) \delta(p_0^2 - E_-^2 - \Delta_{1-}^2) \right]$$

*) The CFL states is similar to the Balian-Wertharmer (BW) state¹⁷⁾ in the following sense. The BW state is characterized by the unit gap matrix in the angular momentum and spin spaces, and has a gap on the whole Fermi surface. On the other hand, the CFL state is also a diagonal unit matrix in the color-flavor $\bar{\mathbf{3}}_c \times \bar{\mathbf{3}}_f$ space, and this leads non-zero gap for all nine quarks in color and flavor space. The 2SC state is much like to Anderson-Morel (ABM) state¹⁶⁾, or to polar state, which is not diagonal and isotropic state, and has gapless point or line on the Fermi surface.

**) \bar{P}_8 is a square root of the octet projection matrix $(P_8)_{ij}^{ab} = \delta^{ab} \delta_{ij} - \delta_i^a \delta_j^b / N_c$.

$$-(\bar{P}_8)_{ij}^{ab} \left[\gamma_5 \Lambda_+ \Delta_{8+} 2\pi\epsilon(p_0) \delta(p_0^2 - E_+^2 - \Delta_{8+}^2) + \gamma_5 \Lambda_- \Delta_{8-} 2\pi\epsilon(p_0) \delta(p_0^2 - E_-^2 - \Delta_{8-}^2) \right]. \quad (2.17)$$

The condition $p_0^2 - E^2 - \Delta_{1(8)}(p_0, \mathbf{p}) = 0$ defines the dispersions for the $SU(3)_{C+V}$ singlet (octet) quasi-quark excitations in the CFL state.

The Feynman propagator for $T \neq 0$ can be obtained from above spectral densities,

$$S_{F12}(p_0, \mathbf{p}) = -\frac{\gamma_5 \Lambda_+ \hat{\Delta}_+(p_0, \mathbf{p})}{p_0^2 - (|\mathbf{p}| - \mu)^2 - \hat{\Delta}_+^2 + i\eta} - \frac{\gamma_5 \Lambda_- \hat{\Delta}_-(p_0, \mathbf{p})}{p_0^2 - (|\mathbf{p}| + \mu)^2 - \hat{\Delta}_-^2 + i\eta} + i n_F(|p_0|) \epsilon(p_0) \rho_{12}(p_0, \mathbf{p}; \mu). \quad (2.18)$$

$\hat{\Delta}$ and ρ_{12} is color-flavor matrix each for the 2SC and the CFL. n_F is the thermal Fermi distribution function defined by

$$n_F(|p_0|) = \frac{1}{1 + e^{|p_0|/T}}. \quad (2.19)$$

This produces the Pauli-blocking term in the final gap equation by thermal on-shell quarks at finite T , and suppresses the phase space for pairing correlation and brings about the phase transition to normal phase at some critical temperature.

Gap equations for the 2SC and CFL states : Now we simplify the gap equation through the vertex decomposition. In the case of the 2SC, we use the following equation,

$$\sum_{A=1}^8 t_A^t \lambda_2 t_A = -\frac{N_c + 1}{2N_c} \lambda_2. \quad (2.20)$$

In the case of the CFL, we use the following color-flavor algebra,

$$\sum_{A=1}^8 t_A^t (P_1) t_A = \frac{1}{2N_c} (\bar{P}_8), \quad \sum_{A=1}^8 t_A^t (\bar{P}_8) t_A = \frac{N_c^2 - 1}{2N_c} (P_1) - \frac{1}{N_c} (\bar{P}_8). \quad (2.21)$$

These identities can be derived by the Fierz identity :

$$\sum_{A=1}^8 (\lambda_A)_{ab} (\lambda_A)_{cd} = -(2/N_c) \delta_{ab} \delta_{cd} + 2\delta_{ad} \delta_{bc}.$$

Using these identities, we obtain

$$\frac{2N_c}{N_c + 1} \Delta_+ = K^+ [\Delta_+, \Delta_-], \quad \frac{2N_c}{N_c + 1} \Delta_- = K^- [\Delta_+, \Delta_-], \quad (2.22)$$

for the 2SC, and

$$\frac{2N_c}{N_c^2 - 1} \Delta_{1+} = -K^+ [\Delta_{8+}, \Delta_{8-}], \quad 2N_c \Delta_{8+} + \frac{4N_c}{N_c^2 - 1} \Delta_{1+} = -K^+ [\Delta_{1+}, \Delta_{1-}], \quad (2.23)$$

$$\frac{2N_c}{N_c^2 - 1} \Delta_{1-} = -K^- [\Delta_{8+}, \Delta_{8-}], \quad 2N_c \Delta_{8-} + \frac{4N_c}{N_c^2 - 1} \Delta_{1-} = -K^- [\Delta_{1+}, \Delta_{1-}]. \quad (2.24)$$

for the CFL. We define the kernel integral for OGE as:

$$K^\alpha [\Delta_+, \Delta_-] = -ig^2 \int \frac{d^4 q}{(2\pi)^4} \left\{ S_F^+(q; \Delta_+) c_{\mu\nu}(p_{\bar{\alpha}}, q_+) \right. \\ \left. + S_F^-(q; \Delta_-) c_{\mu\nu}(p_{\bar{\alpha}}, q_-) \right\} \mathcal{D}_{\mu\nu}(q_0 - p_0, \mathbf{q} - \mathbf{p}), \quad (2.25)$$

with definition

$$S_F^\pm(q; \Delta_\pm) = \frac{\Delta_\pm}{q_0^2 - (|\mathbf{q}| \mp \mu)^2 - \Delta_\pm^2 + i\eta} \\ + 2\pi i n_F(|q_0|) \delta[q_0^2 - (|\mathbf{q}| \mp \mu)^2 - \Delta_\pm^2]. \quad (2.26)$$

Index α takes $+$ and $-$, and we define $\bar{\alpha} \equiv -\alpha$. These gap equations are the generalization of those obtained in Ref. ⁵⁾ to the non-local interaction in arbitrary N_c with the antiquark gap.

Gluon propagator in the quark Fermi liquid : We use the quasi-static approximation of the hard dense loop propagator in the Landau gauge, as it is taken in Refs. ^{14), 24), 30)}.

$$\mathcal{D}_{\mu\nu}(p_0, \mathbf{p}) = -\Delta_T(p_0, \mathbf{p}) P_{\mu\nu}^T - \Delta_L(p_0, \mathbf{p}) P_{\mu\nu}^L, \quad (2.27)$$

with the transverse and longitudinal projection matrices,

$$P_{ij}^T = \delta_{ij} - \hat{p}_i \hat{p}_j, \quad P_{0i}^T = P_{i0}^T = P_{00}^T = 0, \quad P_{\mu\nu}^L = -g_{\mu\nu} + \frac{p_\mu p_\nu}{p_0^2 - p^2} - P_{\mu\nu}^T, \quad (2.28)$$

and the corresponding amplitudes

$$\Delta_T(p_0, \mathbf{p}) = \frac{1}{p^2 + i\theta(p - p_0)(\pi m_D^2/4)|p_0|/p}, \quad \Delta_L(p_0, \mathbf{p}) = \frac{1}{p^2 + m_D^2}. \quad (2.29)$$

$m_D^2 = N_f g^2 \mu^2 / 2\pi^2$ is the Debye screening mass in the quark-gluon plasma. In magnetic sector, we have to take into account the subleading correction from the dynamical sector up to linear in p_0/p in order to avoid the collinear singularity.^{*)} We have neglected the effect of the temperature on the polarization because our main interest lies in the region $\Delta(\mathbf{p})|_{T=0} \ll \mu$.

Gap equation for quasi-particle on the mass shell : Now we simplify the gap equation by integrating out the frequency as in Ref. ¹⁴⁾ because our main interest lies in the gap of quasi-quarks on the mass shell. In the kernel K^α of the gap equations, we have three contributions: quark pole, plasmon pole and branch cut in the gluon continuum. It has

^{*)} The quasi-static approximation can be justified if the ratio of the obtained gap to the Fermi surface (Δ/μ) is small enough to neglect $(\Delta/\mu)^2$. The quasi-static approximation is going well in our model, because it will turn out $\Delta/\mu \sim 1/10$ even at the lowest density.

been shown in Ref.²⁴⁾ that only the quark pole has a significant effect on gap equations at least in the weak coupling limit $\Delta(\mathbf{p})/\mu \rightarrow 0$ at $T = 0$. Here, we assume this property holds even at finite temperatures and/or in the strong coupling regime. The resulting gap equations for the 2SC and CFL states under quark pole dominance take the same forms as Eqs. (2.22)~(2.24) under replacement of the kernels K^α by :

$$\begin{aligned} \mathbf{K}^\pm[\mathbf{p}; \Delta_\pm] \equiv & \int \frac{d\mathbf{q}}{(2\pi)^3} \mathcal{D}_{\pm+}(\mathbf{p}, \mathbf{q}) \frac{\Delta_+(\mathbf{q})}{2\epsilon_+(\mathbf{q})} \left[1 - 2n_F[\epsilon_+(\mathbf{q})] \right] \\ & + \int \frac{d\mathbf{q}}{(2\pi)^3} \mathcal{D}_{\pm-}(\mathbf{p}, \mathbf{q}) \frac{\Delta_-(\mathbf{q})}{2\epsilon_-(\mathbf{q})} \left[1 - 2n_F[\epsilon_-(\mathbf{q})] \right], \end{aligned} \quad (2.30)$$

where $\epsilon_\pm(\mathbf{p}) = \sqrt{(p \mp \mu)^2 + \Delta_\pm(\mathbf{p})^2}$, and $\Delta_\pm(\mathbf{p})$ are gaps on the quasi-quark and quasi-antiquark on the mass shell. The effective interaction $\mathcal{D}_{\alpha\beta}(\mathbf{q}, \mathbf{p})$ is constructed by the following electric and magnetic interactions,

$$\mathcal{D}_{\alpha\beta}(\mathbf{p}, \mathbf{q}) = \mathcal{D}_{\alpha\beta}^E(\mathbf{p}, \mathbf{q}) + 2\mathcal{D}_{\alpha\beta}^M(\mathbf{p}, \mathbf{q}), \quad (2.31)$$

with

$$\begin{aligned} \mathcal{D}_{+\pm}^E(\mathbf{p}, \mathbf{q}) &= \mathcal{D}_{-\mp}^E(\mathbf{p}, \mathbf{q}) = \frac{g^2(1 \pm \hat{\mathbf{p}} \cdot \hat{\mathbf{q}})/2}{(\mathbf{p} - \mathbf{q})^2 + m_D^2}, \\ \mathcal{D}_{\alpha\pm}^M(\mathbf{p}, \mathbf{q}) &= \frac{1}{4} \text{Re} \left[\frac{g^2((\mathbf{p} - \mathbf{q})^2 \pm (p - \hat{\mathbf{p}} \cdot \mathbf{q})(q - \hat{\mathbf{q}} \cdot \mathbf{p}))}{(\mathbf{p} - \mathbf{q})^4 + i(\pi m_D^2/4)|\epsilon_\alpha(\mathbf{p}) - \epsilon_\pm(\mathbf{q})||\mathbf{p} - \mathbf{q}|} \right. \\ &\quad \left. + \frac{g^2((\mathbf{p} - \mathbf{q})^2 \pm (p - \hat{\mathbf{p}} \cdot \mathbf{q})(q - \hat{\mathbf{q}} \cdot \mathbf{p}))}{(\mathbf{p} - \mathbf{q})^4 + i(\pi m_D^2/4)|\epsilon_\alpha(\mathbf{p}) + \epsilon_\pm(\mathbf{q})||\mathbf{p} - \mathbf{q}|} \right] + iO(g^4). \end{aligned}$$

The Fermi distribution function n_F in Eq. (2.30) represents Pauli blocking by thermally excited quasi-quark and quasi-antiquarks. After integration over angular variables, we obtain the following kernels.

$$\begin{aligned} & \mathbf{K}^\pm(p; \Delta_\pm) \\ &= + \frac{g^2}{16\pi^2} \int_0^\infty dq \frac{q}{k} \tanh\left(\frac{\epsilon_+}{2T}\right) \frac{\Delta_+(q)}{2\epsilon_+(q)} \left\{ \pm \frac{(p \pm q)^2 + m_D^2}{2pq} \ln\left(\frac{(p+q)^2 + m_D^2}{(p-q)^2 + m_D^2}\right) \right. \\ &\quad \left. + \frac{1}{3} \ln\left(\frac{(p+q)^6 + M^4(\epsilon_\pm(p) - \epsilon_+(q))^2}{(p-q)^6 + M^4(\epsilon_\pm(p) - \epsilon_+(q))^2} \cdot \frac{(p+q)^6 + M^4(\epsilon_\pm(p) + \epsilon_+(q))^2}{(p-q)^6 + M^4(\epsilon_\pm(p) + \epsilon_+(q))^2}\right) \right\} \\ &\quad + \frac{g^2}{16\pi^2} \int_0^\infty dq \frac{q}{k} \tanh\left(\frac{\epsilon_-}{2T}\right) \frac{\Delta_-(q)}{2\epsilon_-(q)} \left\{ \mp \frac{(p - q)^2 + m_D^2}{2pq} \ln\left(\frac{(p+q)^2 + m_D^2}{(p-q)^2 + m_D^2}\right) \right. \\ &\quad \left. + \frac{1}{3} \left[\ln\left(\frac{(p+q)^6 + M^4(\epsilon_\pm(p) - \epsilon_-(q))^2}{(p-q)^6 + M^4(\epsilon_\pm(p) - \epsilon_-(q))^2} \cdot \frac{(p+q)^6 + M^4(\epsilon_\pm(p) + \epsilon_-(q))^2}{(p-q)^6 + M^4(\epsilon_\pm(p) + \epsilon_-(q))^2}\right) \right] \right\}, \end{aligned}$$

where we have defined $M^2 \equiv \pi m_D^2/4$. We have neglected the parts with higher angular momenta in the gap function $\Delta(\mathbf{q})$.^{*)} Following Ref. ¹⁴⁾, we replace the coupling g^2 with the momentum dependent effective one $\bar{g}^2(p, q)$ by the Higashijima-Miransky prescription ²¹⁾. In the improved ladder approximation, $\bar{g}(p, q)^2$ is taken to be

$$\bar{g}^2(p, q) = \frac{16\pi^2}{\beta_0} \frac{1}{\ln((p_{\max}^2 + p_c^2)/\Lambda^2)}, \quad p_{\max} = \max(p, q), \quad (2.32)$$

where $\beta_0 = (11N_c - 2N_f)/3$, p_c^2 plays a role of a phenomenological infra-red regulator. We adopt $\Lambda = 400$ MeV and $p_c^2 = 1.5\Lambda^2$ ²¹⁾ for numerical calculations.

2.2. CJT effective potentials for finite temperature

The CJT effective potential ³¹⁾ (The Ward-Lattinger effective potential in the case of non-relativistic fermion) for fermion propagator is given by,

$$\Gamma[\mathbf{S}, \mu] = \frac{1}{2} \left\{ \text{TrLog}[\mathbf{S}] - \text{Tr}[\mathbf{S}\mathbf{S}_0^{-1}] + V[\mathbf{S}] \right\}. \quad (2.33)$$

Here, “TrLog” should be interpreted in the functional sense. In the momentum space, $\mathbf{S}^{-1}(p_0, \mathbf{p}) = \mathbf{S}_0^{-1}(p_0, \mathbf{p}) - \boldsymbol{\Sigma}(p_0, \mathbf{p})$ with $\mathbf{S}_0^{-1}(p_0, \mathbf{p}) = \text{diag.}(\not{p} + \not{\mu}, \not{p} - \not{\mu})$. The overall factor 1/2 in the Eq. (2.33) should be introduced to eliminate the artificial degrees of freedom introduced by the Nambu-Gor’kov 2-component fermion. μ represents explicit μ dependence through the bare propagator and the gluon polarization. $V[\mathbf{S}]$ is a potential functional which contains Feynman diagrams of the skeleton self-energy and one quark propagator S . This is a generating functional of the proper self-energy, namely, the functional derivative of the potential is the self-energy, $\delta V[\mathbf{S}]/\delta \mathbf{S} = \boldsymbol{\Sigma}[\mathbf{S}]$. Now we take one loop approximation for $\boldsymbol{\Sigma}[\mathbf{S}]$, symbolically, written as $\boldsymbol{\Sigma}^{(1)}[\mathbf{S}] = g^2 \boldsymbol{\Gamma}_0 \mathbf{S} \boldsymbol{\Gamma} D$.^{*)} In this case, $\Gamma[\mathbf{S}]$ reduces to

$$\Gamma^{(2)}[\mathbf{S}, \mu] = \frac{1}{2} \left\{ \text{TrLog}[\mathbf{S}] - \text{Tr}[\mathbf{S}\mathbf{S}_0^{-1}] + \frac{1}{2} \text{Tr}[\mathbf{S}\boldsymbol{\Sigma}^{(1)}[\mathbf{S}]] \right\}. \quad (2.34)$$

The saddle point approximation leads to the one loop gap equation : $\delta \Gamma^{(2)}/\delta \mathbf{S} = \mathbf{S}^{-1} - \mathbf{S}_0^{-1} + \boldsymbol{\Sigma}^{(1)}[\mathbf{S}] = 0$. We write the solution of this equation $\bar{\mathbf{S}}(g; \mu)$ and $\mathbf{S}_0^{-1} - \bar{\mathbf{S}}^{-1} \equiv \bar{\boldsymbol{\Sigma}}(g; \mu)$. At the stationary point, we can simplify the effective potential:

$$\Gamma^{(2)}[\bar{\mathbf{S}}(g; \mu), \mu] = \frac{1}{2} \left\{ \text{TrLog}[\bar{\mathbf{S}}] - \frac{1}{2} \text{Tr}[\bar{\mathbf{S}}\bar{\boldsymbol{\Sigma}}] \right\}. \quad (2.35)$$

This is a useful formula in which the coupling and gluon propagator do not appear explicitly, but are hidden in $\bar{\mathbf{S}}$ and $\bar{\boldsymbol{\Sigma}}$. Using CJT method described above, the thermodynamic

^{*)} The gap function $\Delta(\mathbf{q})$ can be expanded as $\Delta(\mathbf{q}) = \Delta(q) + \sum_{l=1}^{\infty} \Delta^l(q) P_l(\cos \theta)$. We assume $\Delta^l \ll \Delta$, because the isotropic gap function can activate the whole Fermi surface where the infrared Cooper singularity lies.

^{*)} $\boldsymbol{\Gamma}_0$ and $\boldsymbol{\Gamma}$ means the bare and full vertices in the Nambu-Gor’kov base.

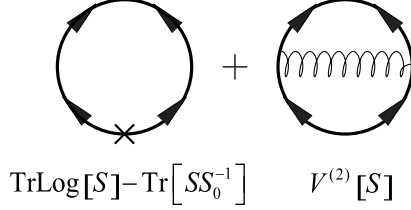


Fig. 1. Schematic Feynman graph of 2-loop CJT potential functional. \mathbf{S} -derivative on this potential is removing one solid line, which yields one loop gap equation.

potential (condensation energy) density relative to the normal Fermi gas up to 2-loop order is given by

$$\delta\Omega(\mu, T) = \frac{1}{\beta V} \left\{ \frac{1}{2} \text{TrLog}[\mathbf{S}\mathbf{S}_0^{-1}] - \frac{1}{4} \text{Tr}[\mathbf{S}\boldsymbol{\Sigma}] \right\}. \quad (2.36)$$

Note that this expression is only valid at the stationary point which can be determined by the gap equation for $\boldsymbol{\Sigma}$. After an involved but straightforward algebra and Matsubara summation, we reach the following expression for the 2SC phase,

$$\begin{aligned} \frac{\delta\Omega_{2\text{SC}}}{6N_c} = & \frac{2}{3} \frac{N_c - 1}{N_c} \left[-T \int \frac{d\mathbf{q}}{(2\pi)^3} \left\{ \ln \left[\frac{\cosh(\epsilon_+/2T)}{\cosh(|E_+|/2T)} \right] + \ln \left[\frac{\cosh(\epsilon_-/2T)}{\cosh(E_-/2T)} \right] \right\} \right. \\ & \left. + \frac{1}{2} \int \frac{d\mathbf{q}}{(2\pi)^3} \left\{ \frac{\Delta_+^2}{2\epsilon_+} \tanh\left(\frac{\epsilon_+}{2T}\right) + \frac{\Delta_-^2}{2\epsilon_-} \tanh\left(\frac{\epsilon_-}{2T}\right) \right\} \right]. \end{aligned} \quad (2.37)$$

Roughly speaking, the first term represents the thermodynamic energy gain by the dynamical quark loop in the presence of the condensate, while the second term represents the energy cost to put the condensate in the Fermi gas. $2(N_c - 1)/3N_c$ in front of right hand side of the above equation indicates that the flavors joining the pairing are 2 out of 3, while the active colors are $N_c - 1$ out of N_c .

In the CFL case, the algebra is more complicated but a straightforward calculation yields the following result,

$$\begin{aligned} \frac{\delta\Omega_{\text{CFL}}}{6N_c} = & -T \int \frac{d\mathbf{q}}{(2\pi)^3} \left\{ \frac{1}{N_c^2} \ln \left[\frac{\cosh(\epsilon_{1+}/2T)}{\cosh(|E_+|/2T)} \right] + \frac{N_c^2 - 1}{N_c^2} \ln \left[\frac{\cosh(\epsilon_{8+}/2T)}{\cosh(|E_+|/2T)} \right] \right\} \\ & -T \int \frac{d\mathbf{q}}{(2\pi)^3} \left\{ \frac{1}{N_c^2} \ln \left[\frac{\cosh(\epsilon_{1-}/2T)}{\cosh(E_-/2T)} \right] + \frac{N_c^2 - 1}{N_c^2} \ln \left[\frac{\cosh(\epsilon_{8-}/2T)}{\cosh(E_-/2T)} \right] \right\} \\ & + \frac{1}{2} \int \frac{d\mathbf{q}}{(2\pi)^3} \left\{ \frac{1}{N_c^2} \frac{\Delta_{1+}^2}{2\epsilon_{1+}} \tanh\left(\frac{\epsilon_{1+}}{2T}\right) + \frac{N_c^2 - 1}{N_c^2} \frac{\Delta_{8+}^2}{2\epsilon_{8+}} \tanh\left(\frac{\epsilon_{8+}}{2T}\right) \right\} \\ & + \frac{1}{2} \int \frac{d\mathbf{q}}{(2\pi)^3} \left\{ \frac{1}{N_c^2} \frac{\Delta_{1-}^2}{2\epsilon_{1-}} \tanh\left(\frac{\epsilon_{1-}}{2T}\right) + \frac{N_c^2 - 1}{N_c^2} \frac{\Delta_{8-}^2}{2\epsilon_{8-}} \tanh\left(\frac{\epsilon_{8-}}{2T}\right) \right\}. \end{aligned} \quad (2.38)$$

Eqs. (2.38) and (2.37) take simple forms $\delta\Omega_{\text{CFL}}(\mu, T)/\mu^4 = f(\Delta_1/\mu) + (N_c N_f - 1)f(\Delta_8/\mu) = f(\Delta_1/\mu) + 8f(\Delta_8/\mu)$ and $\delta\Omega_{2\text{SC}}(\mu, T)/\mu^4 = 2(N_c - 1)f(\Delta/\mu) = 4f(\Delta/\mu)$. Therefore, if the

gaps Δ , Δ_1 and Δ_8 take all the same value, then the condensation energy for the CFL phase is 9/4 times larger than that for the 2SC phase. The comparison of the $(u, d) + s$ 2SC matter with the (u, d, s) CFL phase is not quite obvious till one adopts a model and solves the gap equations and the thermodynamic potential.

2.3. Occupation numbers and Correlation functions

Here we give expressions for various quantities in the ground state.

Quark number density : Occupation number characterizes how much the Fermi sphere is distorted by the gap. We can extract the occupation numbers from the frequency integral of the diagonal propagator $S_{11}(q_0, q)$,

$$n_+^{r,b}(q) = \frac{1}{2} - \frac{E_+}{2\epsilon_+} \tanh\left(\frac{\epsilon_+}{2T}\right), \quad n_-^{r,b}(q) = \frac{1}{2} - \frac{E_-}{2\epsilon_-} \tanh\left(\frac{\epsilon_-}{2T}\right) \quad (2.39)$$

$$n_+^g(q) = (1 - n_F(|E_+|)\theta(-E_+) + n_F(|E_+|)\theta(E_+), \quad n_-^g(q) = n_F(E_-). \quad (2.40)$$

$n_+(q)$ and $n_-(q)$ are distribution functions for quark and antiquark. $n_F(|E_+|)\theta(-E_+)$, $n_F(|E_+|)\theta(E_+)$ and $n_F(E_-)$ represent the thermal hole, the thermal quark and the anti-quark, respectively. Net quark density for the 2SC in some chemical potential μ can be obtained by

$$\rho(\mu) = 4 \int \frac{d\mathbf{q}}{(2\pi)^3} \left[(N_c - 1)(n_+^{r,b}(q) - n_-^{r,b}(q)) + (n_+^g(q) - n_-^g(q)) \right]. \quad (2.41)$$

The chemical potential has to be determined by the number conservation $\rho = \rho(\mu)$, which also can be obtained by the derivative of the pressure $-\Omega(\mu)$.

Similarly, we can find occupation number in the CFL phase as

$$n_{1\pm}(q) = \frac{1}{2} - \frac{E_{1\pm}}{2\epsilon_{1\pm}} \tanh\left(\frac{\epsilon_{1\pm}}{2T}\right), \quad n_{8\pm}(q) = \frac{1}{2} - \frac{E_{8\pm}}{2\epsilon_{8\pm}} \tanh\left(\frac{\epsilon_{8\pm}}{2T}\right). \quad (2.42)$$

n_1 and n_8 are the color-flavor singlet and octet distribution, which can be defined using the annihilation operator for quark, $a(p)$ and that for antiquark $b(p)$ as

$$\begin{aligned} \langle a_i^{a\dagger}(p) a_j^b(p) \rangle &= (P_1)_{ij}^{ab} n_{1+}(p) + (P_8)_{ij}^{ab} n_{8+}(p), \\ \langle b_i^{a\dagger}(p) b_j^b(p) \rangle &= (P_1)_{ij}^{ab} n_{1-}(p) + (P_8)_{ij}^{ab} n_{8-}(p). \end{aligned}$$

Using these octet and singlet densities, we find by putting $b = a$ and $j = i$ in the above equation,

$$n_{i\pm}^a(q) = n_{8\pm}(q) + \delta_i^a \frac{1}{N_c} \left[n_{1\pm}(q) - n_{8\pm}(q) \right]. \quad (2.43)$$

$n_i^a(p)$ is the probability distribution finding a quark (+) or an antiquark (−) with color a and flavor i having the momentum p . We can see the fact that the quark density is almost determined by the octet density. The total quark numbers for quark and antiquark read

$$\rho(\mu) = 2 \int \frac{d\mathbf{q}}{(2\pi)^3} \left[(N_c N_F - 1)(n_{8+}(q) - n_{8-}(q)) + (n_{1+}(q) - n_{1-}(q)) \right]. \quad (2.44)$$

Correlation functions : What is important to characterize a superconducting phase is a energy gap and the correlation functions which describes the off-diagonal long range order in the system. This quantities are also called the anomalous density because it is related to the anomalous propagators $\langle Tqq \rangle$. In the case of the 2SC,

$$\phi_{\pm}(q) = \tanh\left(\frac{\epsilon_{\pm}}{2T}\right) \frac{\Delta_{\pm}}{2\epsilon_{\pm}} = \left[1 - 2n_F(\epsilon_{\pm})\right] \frac{\Delta_{\pm}}{2\epsilon_{\pm}}. \quad (2.45)$$

Here, the correlation functions $\phi_{\pm}(p)$ are defined by

$$\langle a_i^a(p) a_j^b(-p) \rangle = (\tau_2 \lambda_2)_{ij}^{ab} \phi_+(q), \quad \langle b_i^a(p) b_j^b(-p) \rangle = (\tau_2 \lambda_2)_{ij}^{ab} \phi_-^*(q).$$

To avoid an involved notation, we have omitted the helicity indices. As is postulated for the ansatz of the 2SC condensate, the correlation exists only in the color-flavor anti-symmetric channel. The minus sign in front of n_F in Eq. (2.45) shows the effect that the thermally excited quasi-particles reduce the strength of the correlation.

In the same way as in the 2SC case, we easily derive the correlation functions in the CFL phase, The anomalous densities in the singlet and octet channels become

$$\phi_{1\pm}(q) = \tanh\left(\frac{\epsilon_{1\pm}}{2T}\right) \frac{\Delta_{1\pm}}{2\epsilon_{1\pm}}, \quad \phi_{8\pm}(q) = \tanh\left(\frac{\epsilon_{8\pm}}{2T}\right) \frac{\Delta_{8\pm}}{2\epsilon_{8\pm}}. \quad (2.46)$$

with definition

$$\begin{aligned} \langle a_i^a(p) a_j^b(-p) \rangle &= (P_1)_{ij}^{ab} \phi_{1+}(q) + (\bar{P}_8)_{ij}^{ab} \phi_{8+}(q), \\ \langle b_i^a(p) b_j^b(-p) \rangle &= (P_1)_{ij}^{ab} \phi_{1-}^*(q) + (\bar{P}_8)_{ij}^{ab} \phi_{8+}^*(q). \end{aligned}$$

By using the locking relation $\epsilon_{Iab} \epsilon_{ij}^I = (N_c - 1)(P_1)_{ij}^{ab} - (\bar{P}_8)_{ij}^{ab}$, the color $\bar{\mathbf{3}}_c$ flavor antisymmetric correlation $\phi_A(q)$ and the color $\mathbf{6}_c$ and flavor symmetric correlation $\phi_S(q)$ are extracted as

$$\phi_A(q) = \frac{1}{N_c} \phi_{1\pm}(q) - \left(1 + \frac{1}{N_c}\right) \phi_{8\pm}(q), \quad \phi_S(q) = \frac{1}{N_c} \phi_{1\pm}(q) + \left(1 - \frac{1}{N_c}\right) \phi_{8\pm}(q).$$

We would see ϕ_S disappears rapidly near the critical temperature compared with ϕ_A , due to anti-triplet dominance in the critical region.

§3. Numerical results

In this section, we present our numerical results. First, we focus on how the temperature affects the superconducting gap, and other physical quantities at a high chemical potential $\mu = 1000$ MeV. We discuss various features of the phase transition. Then, we see how these pictures of the phase transition would be modified towards low, physically interesting densities. Finally, we draw the QCD phase diagram for the region $\mu \gtrsim 400$ MeV. We estimate the effect of the effective strange quark mass m_s on the QCD phase diagram using a simple unlocking criterion, and study how the QCD phase diagram changes with a variation of m_s .

3.1. Phase transitions to QGP phase at $\mu = 1000$ MeV

Gap functions and condensation energies : We show the numerical solutions for the gap equations Eqs. (2.22)~(2.24) at a fixed chemical potential $\mu = 1000$ MeV corresponding to about 80 times the normal nuclear density $\rho_0 = 0.17 \text{ fm}^{-3}$. Fig. 2 shows the gap function $\Delta_{\pm}(p)$ for the 2SC state (a), and the singlet and octet gap functions ($\Delta_{1\pm}(p)$, $\Delta_{8\pm}(p)$) for the CFL state (b). At first sight, we can see the shapes of these gap functions are all similar as a function of momentum except for the magnitude $|\Delta_8(p)| < |\Delta(p)| < |\Delta_1(p)|$ and the relative sign between the singlet and octet gaps. Secondly, we observe the temperature uniformly reduces the magnitudes of the gap functions towards the critical temperature which can be read ~ 15 MeV.

In order to see characteristics of phase transitions in more detail, we show in Fig. 3, the temperature dependence of the gaps at Fermi surface (a) and that of the CJT condensation energies for the 2SC and CFL states (b). From these figures, we can see that the phase transitions to the QGP phase both from the 2SC state and from the CFL phase are of 2nd order just like in the BCS theory with contact interaction : The derivatives of the gaps seem to diverge towards the T_c in (a), and thermodynamic bulk quantities in superconducting phases are connecting continuously to those of normal QGP phase (b). Another thing to be noticed is that the critical temperatures to the QGP phase are the same both for the CFL and for the 2SC. We will discuss this property in more detail latter in this section and see that this holds at least in the weak coupling limit.

The condensation energy for the CFL state is always about 1.9~ 2 times larger than that for the 2SC in spite of the fact that the octet gaps determining the thermodynamics in the CFL takes smaller values than the 2SC gaps. This is consistent with the weak coupling analytical estimate¹³⁾ : The CFL phase is easier to excite quasi-quarks, but the bulk energy is lower in the CFL than in the 2SC. This reversal between the condensation energy and the magnitude of gap is clearly a direct consequence of the fact that the number of the active

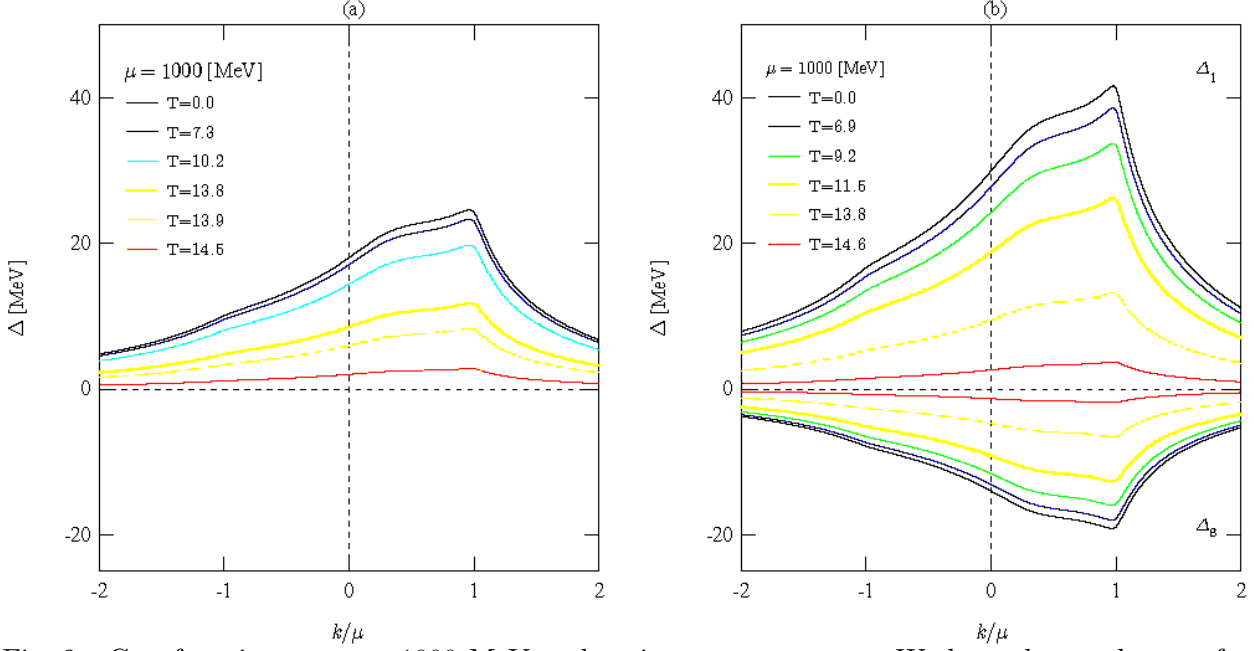


Fig. 2. Gap functions at $\mu = 1000$ MeV and various temperatures. We have drawn the gap for antiquarks at negative momentum region, namely, $(-|k|, \Delta_- (|k|))$ are plotted at left half of the figure. (a) Gap function for the 2SC state. (b) Gap functions for the CFL state.

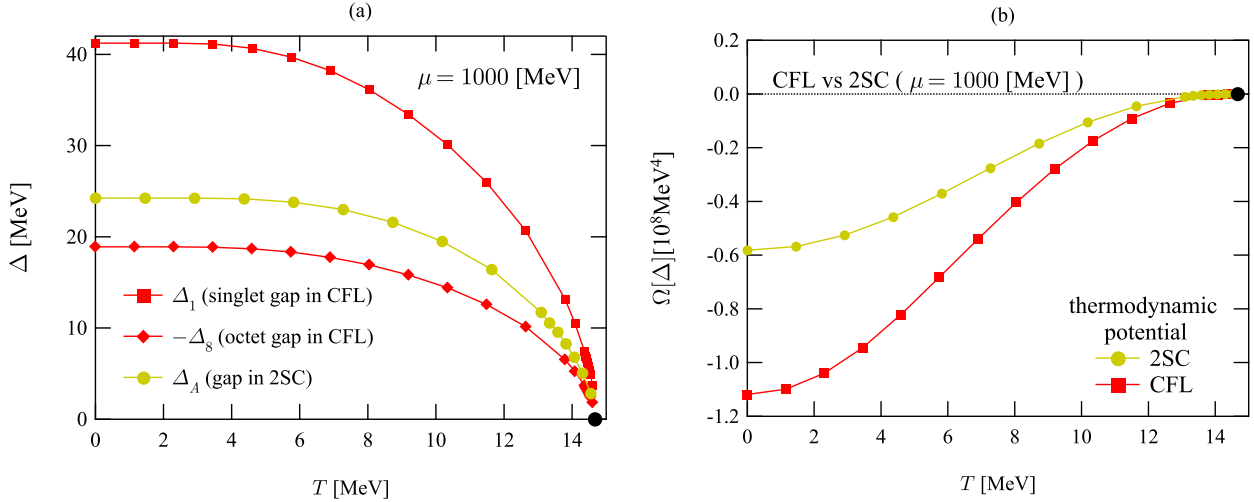


Fig. 3. CFL vs. 2SC.

(a) Gaps at the Fermi surface vs. temperature. (b) Thermodynamic potential and energy gain per quark for both phases at $\mu = 1000$ MeV.

freedom taking part in pairing is 9/4 times larger in the CFL phase than in the 2SC phase^{*)}

^{*)} The condensation energy for the CFL is a function of $\Delta_1^2 + 8\Delta_8^2 \sim 12\Delta_8^2$, and that for the 2SC is a function of $4\Delta^2$. Thus, the thermodynamic enhancement factor 9/4 is a little bit underestimated, but is enough for explaining the CFL dominance at $T = 0$.

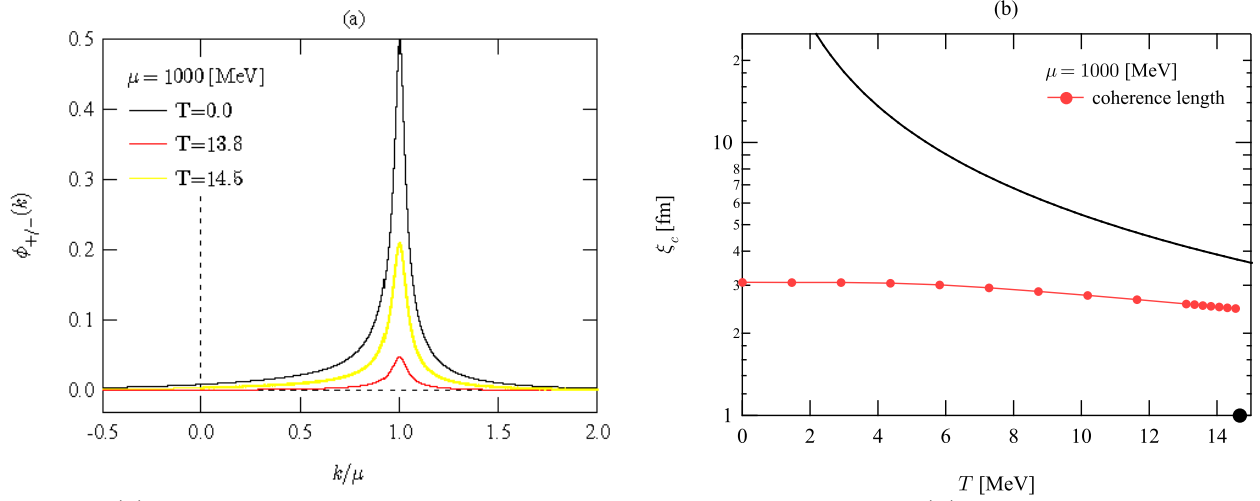


Fig. 4. (a) Correlation functions for the 2SC at finite temperature. (b) The coherence length and the Pippard length in the 2SC state. Black line show the thermal wave length of the un-perturbed Fermi gas $\sim 1/2T$.

It can be said that the CFL state is relatively more fragile.^{*)} than the 2SC state due to smaller gap in the color-flavor octet channel. Reflecting this, the critical temperatures to the QGP phase from both states are almost the same although the condensation energy for the CFL at $T = 0$ is 1.9 times larger than that for the 2SC state.

Cooper pair size at $\mu = 1000$ MeV : In Fig. 4(a), the correlation functions for the 2SC at various temperature are shown. These quantities characterize the internal structure of pairs. Although the magnitude of the correlation gets significantly reduced by temperature, the width of the function seems not so much affected. This implies that thermally excited quasi-quarks destroy the phase coherence of the system, but does not change the internal structure of pairs. This fact gives us a picture of the phase transition : The phase transition occurs by the reduction of the number of coherent pairs, not by the dissociation of them. In order to make sure of this point, we have drawn various length and those dependence on temperature in Fig. 4(b). As is speculated above, the coherence length ξ_c denoted by black points are not much affected by temperatures. ξ_c is defined by the root mean square radius of the Cooper pair with wave function ϕ_+ . Black line shows $1/2T$, which is related to the thermal de Broglie wavelength of the naive Fermi gas : $\lambda_T = 1/\sqrt{\langle E_+^2 \rangle_T} \sim 1/2T$. Only the interaction with the length scale $\lesssim \lambda_T$ can cause quantum corrections to the naive

^{*)} Because the quasi-quarks contribution to the thermodynamic quantities in the CFL can be expressed as the integral of $8e^{-\epsilon_8/T} + e^{-\epsilon_1/T}$, the color-flavor singlet quarks with the large gap do not give a significant thermal effect for $T \lesssim T_c$. On the other hand, in the 2SC state, thermal quark contribution to the thermodynamic quantities can be written as the integral of $4e^{-\epsilon/T}$. Thus, the CFL state is more sensitive to temperature than the 2SC state because of octet quasi-quarks with the smallest gap.

Fermi gas. Phase transition to the QGP phase takes place at these 2 length scale becomes comparable, because the quantum correlation with length ξ_c gets gradually destroyed by thermal disturbance with length λ_T .

Why critical temperatures coincides? : Now, we return to the problem why the critical temperatures to the QGP phase coincides. It is related to the disappearance of nonlinear effects near critical temperature T_c . To see this, we rewrite the CFL gap Eqs. (2.23)~(2.24) in terms of the symmetric and anti-symmetric self-energy (Δ_A , Δ_S) in Eq. (2.16). If we neglect the Δ_S term in the loop integral in Eqs. (2.23) and (2.24) (ansatz of the anti-triplet dominance $|\Delta_S| \ll |\Delta_A|$), and also the contribution from antiquarks which can be justified only in the weak coupling region, equations for Δ_A and Δ_S cast into the following form:

$$\frac{4N^2}{N+1}\Delta_A = (N+1)K^+[\Delta_A] + K^+[(N-1)\Delta_A], \quad (3.1)$$

$$\frac{4N^2}{N-1}\Delta_S = (N-1)K^+[\Delta_A] - K^+[(N-1)\Delta_A]. \quad (3.2)$$

If we neglect the nonlinear terms in Δ_A , we obtain

$$\frac{4N^2}{N+1}\Delta_A = 2NK^+[\Delta_A], \quad \frac{4N^2}{N-1}\Delta_S = 0. \quad (3.3)$$

These two “*gap equations*” are consistent with the first ansatz of omitting Δ_S in the loop integral. Discarding nonlinear terms in Δ_A is justified near the critical temperature of the 2nd order transition. To make sure of the validity of this argument, we check the ansatz of the color anti-triplet dominance near the critical temperature. Fig. 5(a) shows correlation functions in the anti-triplet and sextet channels. The sextet correlation disappears rapidly towards the critical point compared to the anti-triplet correlation. Similarly, Fig. 5(b) shows the temperature dependence of the ratio $-\Delta_8/\Delta_1$. This quantity approaches 1/2 near the critical temperature, which directly means the anti-triplet dominance $\Delta_S/\Delta_A \rightarrow 0$ with $T \rightarrow T_c$. The convergence $-\Delta_8/\Delta_1 \rightarrow 1/2$ seems linear in $t = (T_c - T)/T_c$, therefore, if $\Delta_A(t) \cong -\Delta_8(t) \sim t^{1/2}$ near T_c just as the scaling in the mean field approximation, then Δ_S approaches 0 as $\Delta_S \sim t^{3/2}$ towards T_c . Namely, Δ_S disappears rapidly towards T_c .

3.2. Gaps, condensation energies and critical temperatures for $\mu = 1000 \sim 400$ MeV

Now we turn to the axis of chemical potential in the phase diagram, and investigate how the physical quantities studied above change, and how the picture of phase transition gets modified as one goes to lower density ($\mu < 1000$ MeV) region.

Gaps and energy gains per quark at $T = 0$: We show the chemical potential dependence of the 2SC gap Δ and the CFL octet gap $|\Delta_8|$ in Fig. 6(a). The ordering $|\Delta_8| < \Delta$ is true

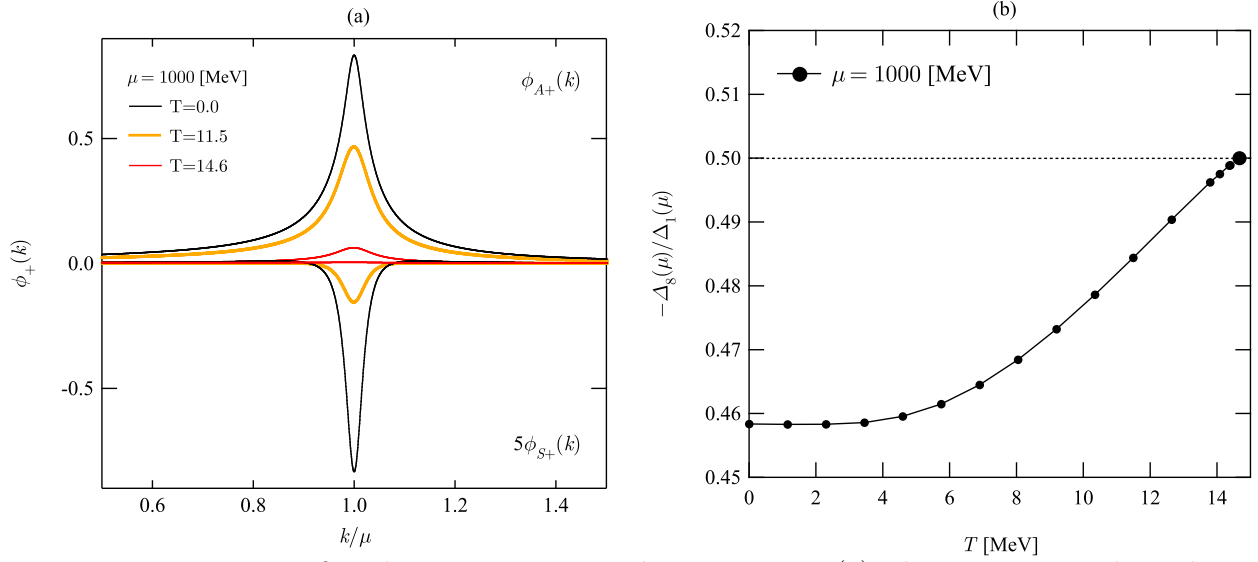


Fig. 5. Disappearance of nonlinearity near critical temperature. (a) The temperature dependence of correlation functions in the anti-triplet and sextet channels for the CFL state. (b) The temperature dependence of the ratio $-\Delta_8/\Delta_1$.

for all region $300 \text{ MeV} < \mu < 1000 \text{ MeV}$. Our gaps have several features which are quite different from those obtained in Ref. ⁵⁾.

(1) The gaps in Ref. ⁵⁾ disappear for $\mu > 800 \text{ MeV}$. Because the NJL model used in the reference is an effective theory originally introduced to describe the chiral symmetry breaking in the QCD vacuum, it has a cut-off scale $\Lambda \sim 1 \text{ GeV}$. Our gaps are also decreasing functions of μ , but do not go to zero even at high density. Furthermore, our gaps will turn into increasing functions of μ at some higher chemical potential $m\mu > 1000 \text{ MeV}$, because our model coincide with other perturbative SD approaches^{32), 25), 26), 24)}, which all predict increasing gaps in the weak coupling regime.

(2) The gaps obtained in Ref. ⁵⁾ go to zero towards $\mu \rightarrow 0$, while our gaps do not. Gap equation at $\mu = 0$ is the same as the chiral gap equation under the replacement the NJL 4-Fermi coupling $K \rightarrow K/2$, if we neglect the small admixture of the pairing correlation in the color and flavor sextet channels. The coupling K has been tuned to reproduce the chiral gap 400 MeV at zero density. Therefore, the disappearance of the superconducting gap at $\mu = 0$ means that $K/2 < K_c < K$, where K_c is the critical coupling for the dynamical generation of the chiral mass gap. On the other hand, our gaps increase as $\mu \rightarrow 0$ and seem to converge to non-zero finite values. It can be said that our model describes a strong coupling superconductor at low densities in the sense that the large effective coupling constant leads non-zero gaps even in the absence of the Fermi surface¹⁴⁾. Of course, if we had included the diagonal self-energy part which is relevant to the chiral symmetry breaking, then one would

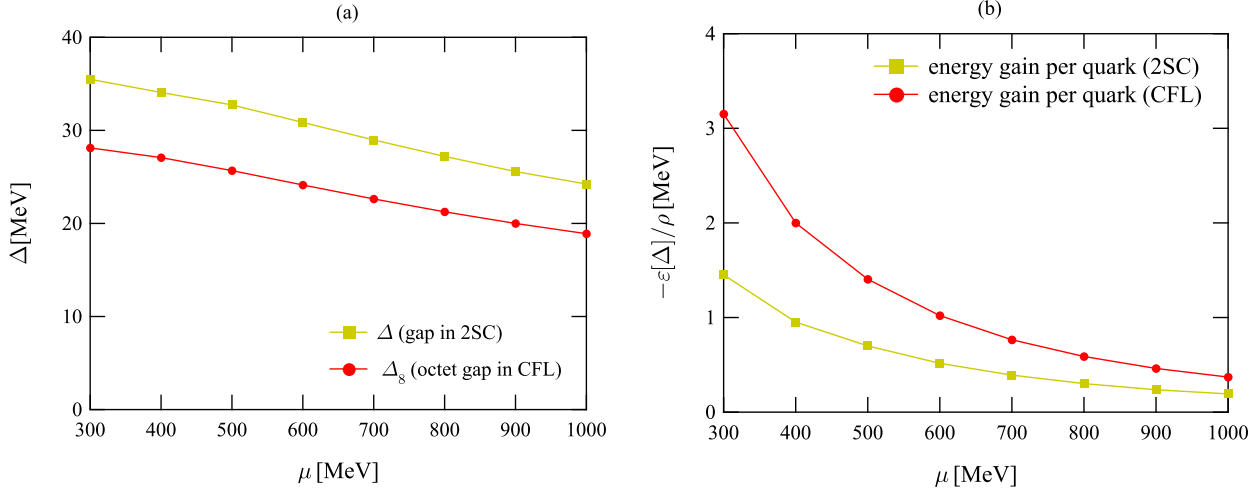


Fig. 6. 2SC vs. CFL at various densities. (a) Chemical potential dependence of the octet gap and the 2SC gap. (b) Density dependence of condensation energy gain per quark both for the CFL and 2SC states.

encounter the phase transition to chiral broken phase at some critical chemical potential μ_c , and the superconducting gap would disappear at zero density due to the reduction of the state density at Fermi surface owing to the generation of mass gap^{33)–35)}.*)

In Fig. 6(b), the chemical potential dependence of the energy gain per quark relative to the naive Fermi gas is shown. First, the CFL state persists against the 2SC for all density region, and its energy gain is about 1.9 times larger than that in the 2SC. Second, this quantity also shows an increasing behaviour as one goes to lower density region. Nevertheless, it is small in order of ~ 1 MeV even at $\mu = 300$ MeV. This fact is attributed to the fact that particle energy gain is proportional to $\sim \Delta(\Delta/\mu)$, namely, the pairing effect on the energy gain per quark is suppressed by factor Δ/μ . This means that only Δ/μ of total quarks near the Fermi surface get the energy gain $-\Delta$. However, $\Delta/\mu \sim 1/10$ at $\mu = 300$ MeV is quite larger than the case of the BCS weak coupling superconductor, where typically this ratio takes the value $\sim 1/1000$. It can be said that the color superconductor which might be realized in the neutron star core is high T_c one of strong coupling.

Critical temperatures : Now we discuss the chemical potential dependence of the critical temperature. In Fig. 7 (a), critical temperatures for the 2SC and CFL states as a function of the quark chemical potential are shown. The dependence of T_c on the chemical potential is similar to those of gaps in Fig. 6(a). The strong coupling effects also exist and lift up critical temperatures at lower densities. Even then, the critical temperature at the lowest density is ~ 20 MeV. Although the behaviour of the critical temperature as a function of

*) However, there is a model in which the diquark gap persists against the sudden jump of the chiral gap³⁶⁾.

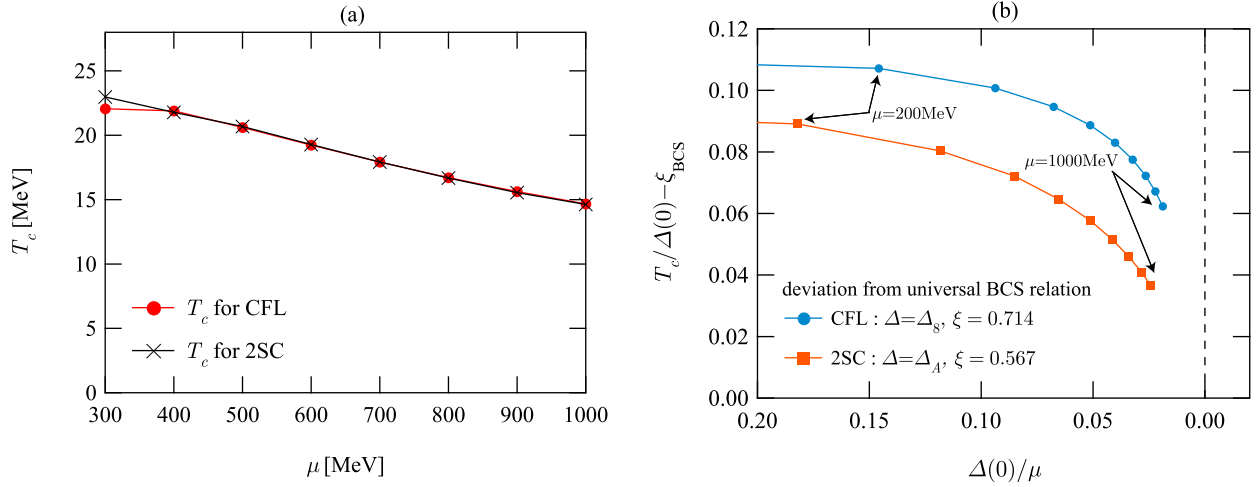


Fig. 7. (a) Critical temperatures extracted by fitting the data in the from $\Delta(T) = \alpha(T_c - T)^\beta$, vs. chemical potential (b) The deviations of the ratio $T_c(\mu)/\Delta(\mu, T = 0)$ from its weak coupling universal value ξ , vs. Δ/μ , a variable for the weak coupling expansion.

μ is qualitatively similar to that obtained from the improved SD approach for $m_s = \infty$ in the Ref. ²⁰⁾, the magnitude of the critical temperature is much smaller in our case than ~ 150 MeV in the reference. The correct treatment of the Landau damping in the magnetic gluon would make this difference smaller. Fig. 7(b) shows the ratio $T_c(\mu)/\Delta(\mu, T = 0)$ as a function of $\Delta(\mu, T = 0)/\mu$. This ratio takes the coupling independent universal value in the weak coupling limit $\Delta/\mu \rightarrow 0$ in the BCS model with a contact interaction. We can see that this ratio approaches to the weak coupling value towards $\Delta/\mu \rightarrow 0$. However our interested region is far away from the region where the convergence to the weak coupling values can be seen. Again, we notice the importance of the strong coupling effects.

Even in the presence of these strong coupling effects at low densities, the ratio of the critical temperatures for the CFL and 2SC states do not deviate from its weak coupling value. Namely, the critical temperatures for the 2SC state coincides with that for the CFL state for all region of chemical potential within numerical errors.

Simple estimate of the unlocking transition for $T = 0$: Here we estimate the color-flavor unlocking transition at $T = 0$ using a simple kinematical criterion, which turned out to be quite a good guide for unlocking transition in the NJL-like model analyses ^{10), 11)}. In Fig. 8, we have shown the critical strange quark mass in a kinematical criterion which can be extracted from our result for the unperturbed octet gap as $m_s^c(\mu) = 2\sqrt{\mu\Delta_8(\mu)|_{m_s=0}}$. Suppose that the effective strange quark mass $m_s(\mu)$ is decreasing function of the chemical potential μ . If $m_s(300 \text{ MeV}) > m_s^c(\mu)$ and $m_s(1000 \text{ MeV}) < m_s^c(\mu)$, then $m_s(\mu)$ intersects the curve of $m_s^c(\mu)$ at some point μ_c locating between $300 \text{ MeV} < \mu < 1000 \text{ MeV}$. In the

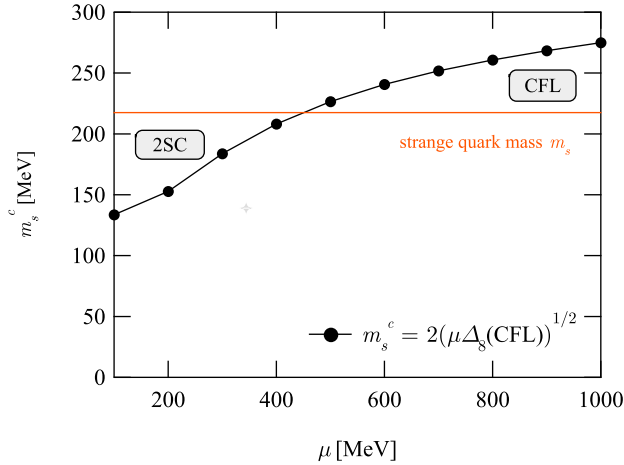


Fig. 8. The chemical potential dependence of the critical strange quark mass from a simple criterion for the unlocking transition with $\Delta_8(\mu)$ obtained by solving the CFL gap equations.

simplified (kinematical) picture, the unlocking transition occurs when the chemical potential μ gets smaller than this μ_c , where the deviation of the Fermi momentum for strange quark from those for light flavors, $p_F^s - p_F^{u,d} = \sqrt{\mu^2 - m_s(\mu)^2} - \mu \sim m_s(\mu)^2/2\mu$, exceeds twice of the smallest gap $|\Delta_8|$ in the CFL state. Here, we had better mention that if we take into account the dynamical effect of the strange quark mass on the formation of gaps, then the gap of quarks belonging to color-flavor octet splits into 4 different values, and the smallest one Δ_s^8 at the critical point sets the true unlocking critical mass $m_s^c(\text{true}) = 2\sqrt{\mu\Delta_s^8}$. In the Ref. ¹¹⁾, the deviation of the smallest gap from the unperturbed octet gap Δ_8 is about 20% at $\mu = 400$ MeV. Thus using the simple kinematical criterion, we might overestimate the critical mass about $100(1 - \sqrt{0.8})/\sqrt{0.8} \sim 10\%$ of the real value for $\mu = 400$ MeV.

In the following, we assume that this criterion is useful even for finite temperature, and we put the further ansatz that the effective mass of the strange quark at chemical potential μ can be approximated to constant $m_s(\mu) = m_s$ for region $300 \text{ MeV} < \mu < 1000 \text{ MeV}$. Instead of this simplified ansatz, we treat m_s as a parameter, change it by hand, and discuss the qualitative dependence of the phase diagram on m_s .

3.3. Phase diagram and its m_s -dependence

Here, we draw a phase diagram expected to be realized from $\mu \sim 300 \text{ MeV}$ to $\mu = 1000 \text{ MeV}$ for various values of the strange quark mass. As already noted above, we consider constant effective strange masses without μ -dependence. Fig. 9 shows our result of the QCD phase diagrams for four values of the strange quark mass $m_s = 0, 150, 200$ and 250 MeV .

1. *The chiral limit $m_s = 0$* : In the chiral limit $m_s = 0$, there is only one line (black bold dot) which divides the (μ, T) plane into the QGP and CFL phases by the 2nd order transition.

This degenerates in double lines, namely, one separating the QGP and the CFL, and the other dividing the QGP and the 2SC. However as we discussed above, the 2SC phase does not appear for $m_s = 0$, because the condensation energy of the CFL is about twice larger than that of the 2SC for all region $T < T_c(\mu)$.

2. $m_s = 150 \text{ MeV}$: We study what happens if we switch on the strange quark mass $m_s = 150 \text{ MeV}$. We estimate this using the kinematical criterion described at the end of the previous section. New line denoted by triangle-line appears in the phase diagram. We call this *color-flavor unlocking critical line*. This unlocking line divides the superconducting region $T < T_c(\mu)$ into the CFL and 2SC phases by 1st order transition. Above this unlocking critical line, the system is unlocked into the 2SC state, and below it, the system stays in the CFL phase. On the unlocking critical line, the pressure for the CFL coincides with that for the 2SC. The strength of the 1st order phase transition gets weaker and weaker towards $\mu \rightarrow \infty$, because the gap between energy density for the 2SC phase and that for the CFL phase gets smaller as one goes near the unlocking line. The critical end point at which the 1st order transition terminates is located at $\mu = \infty$ as long as we use a kinematical criterion, but the dynamical effect of the strange quark mass on the pairing may bring this point to the finite density point. Indeed, in the NJL model analysis¹²⁾, the tricritical point appears at $\mu \sim 520 \text{ MeV}$, although the physical reason of the appearance of 2nd order phase transition has not yet been understood. Furthermore, because this tricritical point is quite close to the cut-off $\Lambda \sim 600 \text{ MeV}$, it might be an artifact of such an effective model with a cut-off scale.

3. $m_s = 200 \text{ MeV}$: Now, we change the strange quark mass $m_s = 150 \text{ MeV}$ to $m_s = 200 \text{ MeV}$. Then the unlocking critical line shifts from the “triangle-line” to the “square-line”. The room for the 2SC realization is enlarged, pushing the CFL area to higher density and lower temperature region. Here we assume the chiral transition occurs near $\mu = 400 \text{ MeV}$, then at zero temperature, the system is always chirally broken by the $q\bar{q}$ condensate for $\mu < 400 \text{ MeV}$, and by the CFL type qq condensate for $\mu > 400 \text{ MeV}$. In this situation $m_s < 200 \text{ MeV}$, quark-hadron continuity might possibly realize.

4. $m_s = 250 \text{ MeV}$: Finally, the “cross-line” represents the unlocking critical line for $m_s = 250 \text{ MeV}$. In this case, the 2SC might intrude into the opening region between the chirally broken vacuum phase and the CFL phase in $T = 0$ section in the QCD phase diagram. Quark-hadron continuity does not occur for $m_s > 250 \text{ MeV}$ in our model. The critical mass for the quark-hadron continuity lies in the interval $200 < m_s^{\text{cont}} < 250 \text{ MeV}$ in our model. The dynamical effect of the strange quark mass on the pairing gap would bring this mass to lower densities. The true critical mass m_s^{cont} from our model would be a little bit smaller

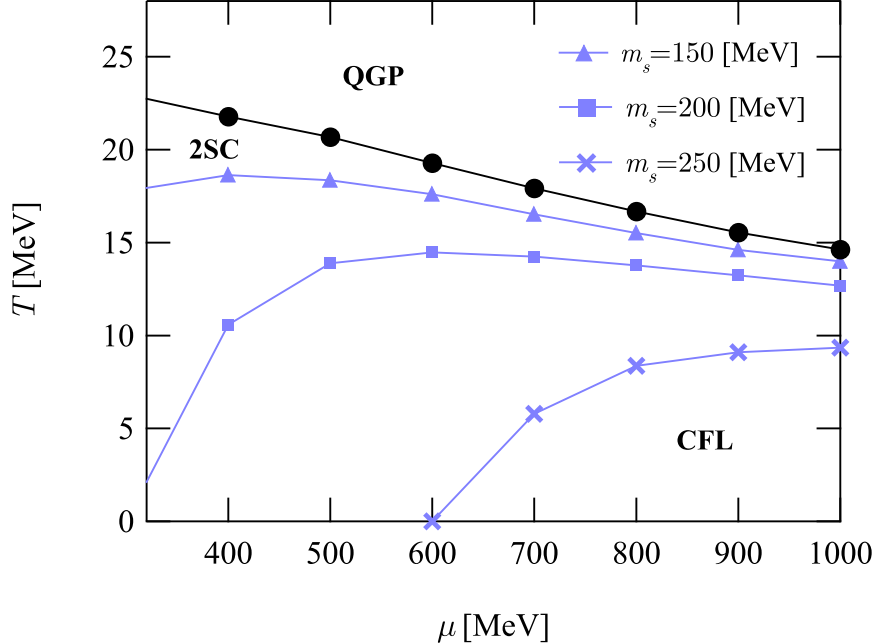


Fig. 9. The QCD phase diagram for various values of the strange quark mass. The bold-dot-line represents the phase boundary between 2SC and QGP separated by the 2nd order phase transition. Triangle-line, square-line and cross-line are showing the gradual change of the unlocking critical line when we shift the strange quark mass as $m_s = 150, 200$ and 250 MeV by hand.

than ~ 250 MeV obtained from the NJL model in Ref. ¹¹).

§4. Summary and Discussion

We have applied the Schwinger-Dyson equation in the improved ladder approximation to the color superconducting phenomena in high density quark matter. Special attention has been given to the competition between the 2SC phase and the CFL phase at finite temperature, and to the effect of the strange quark mass on the QCD phase diagram.

Sec. 2 was devoted to the technical details to obtain the gap equations and the CJT potentials for CFL and for 2SC from the Nambu-Gor'kov Schwinger-Dyson approach. In Sec. 3, we studied which ordering of (2SC, CFL) is favored at relatively low density $\mu = 300 \sim 1000$ MeV at finite temperature. We have drawn the picture of the phase transition by investigating the μ/T dependence of the gap function, the correlation function and the coherent length, as well as bulk quantities such as pressure. We summarize our main results in this paper below.

(1) The phase transitions to the normal phase both from the 2SC and from the CFL have shown almost the same characteristic behaviour as in the BCS weak coupling superconductor

with contact interaction. The critical temperatures for the CFL and the 2SC coincides with each other due to the color anti-triplet dominance, despite the fact that the condensation energy density is almost twice larger in the CFL than in the 2SC. This facts are consistent with weak coupling estimates, and are indicating that the CFL state is more fragile than the 2SC state against thermal fluctuations, due to the smaller energy gap in the color-flavor octet channel. Phase transition occurs as a consequence of the reduction of the coherent Cooper pairs, but not due to the dissociation of those.

(2) The strong coupling effects get larger towards the lower density side. Especially, this was observed in the violation of the universal relation between the gap at $T = 0$ and the critical temperature. This value deviates from the weak coupling analytical value $\sim 15\%$ at $\mu = 300$ MeV. This deviation comes from strong coupling effects, the large off-Fermi surface effect including the pairing in the antiquark channel owing to a larger coupling at lower densities. We find that physically interesting densities lie far away from the region where this ratio seems to converge to the universal value. Despite these strong coupling effects, the ratio of the physical quantities in the CFL state and in the 2SC state, does not so much differ from the weak coupling value even in the strong coupling region.

(3) The QCD phase diagram and the effect of the strange quark mass m_s on it are studied within a simple unlocking criterion. In the chiral limit, there is no room for the 2SC realization, but the finite strange quark mass makes a unlocking critical line separating the superconducting (μ, T) area into the 2SC phase and the CFL phase, and this line push the CFL region to higher density and lower temperature region. The critical end point on which the 1st order unlocking line terminates is located at $\mu = \infty$ as long as a simple kinematical criterion is used. We find a possibility that for $m_s < 200$ MeV, the chiral broken vacuum phase might continuously connected with the CFL phase at high density without any phase transition.

There are several future problems to be studied.

Dirac mass function and chiral condensate : In order to study the phase boundary region where the chiral restoration occurs, we have to include the diagonal self-energy in our SD equation. Within the 4-Fermi contact interaction model, the competition between the chiral condensate and diquark condensate is investigated by several authors^{33), 34)}. Also, the SD approach is examined in Ref.²⁰⁾ for $m_s = \infty$. In particular, the $s\bar{s}$ condensate, or equivalently, the dynamical strange quark mass is shown to play an important role for the phase boundary between the 2SC and the CFL¹⁰⁾, which strongly stabilizes the 2SC phase with finite strange quark mass. The critical strange quark mass for unlocking transition may be significantly lowered by this effect^{10), 12)}.

Wavefunction renormalization and chemical potential renormalization : There is an infrared singular factor in the fermion wavefunction renormalization : $Z^{-1}(k_0) = 1 + \text{const.} g^2 \log(\mu/q_0)$ at the one loop level³⁷⁾. Furthermore, the chemical potential also suffers from a renormalization because if $\mu \neq 0$, Lorentz symmetry is explicitly broken down to $O(3)$. The full self-consistent treatment of both the gap, Z^{-1} and a chemical potential renormalization μ_r is needed for more quantitative argument.

Exact treatment of the strange quark mass : In this paper, the effect of the strange quark mass was examined within a simple kinematical criterion. It would be interesting to examine the full treatment at finite temperature in our improved SD approach³⁸⁾. So far, the unlocking phase transition at finite temperature has not yet studied in a perfect way. Including the dynamical effect of the strange quark mass on the gaps, we can make sure whether the critical end point might show up at finite chemical potential or not, namely the end-point obtained in Ref.¹²⁾ is an artifact of an effective model with cut-off or not.

Electric charge and color neutrality : Imposing the color and the electric charge neutrality has been shown to strongly disfavor the 2SC by the model independent analysis by Alford and Rajagopal³⁹⁾. Their argument based on the weak coupling expansion of thermodynamic potential in $\Delta \sim m_s^2/\mu$ reveals that the 2SC state hardly realizes in the neutron stars. Several works^{40)–42)} also show that the naive 2SC phase costs the large energy for enforcing the neutrality. It would be interesting to examine our improved SD approach to the neutral quark matter, and to determine the phase diagram under neutral condition.

Another possibility of the ground state : As long as we restrict ourselves to the homogeneous system, the unlocking transition is unique for a given chemical potential μ , and thus the m_s dependent unlocking critical line appears in the phase diagram. However, if we remove this restriction, then this line might split into two lines and another inhomogeneous state like the LOFF state^{43), 44)} might intrude between the CFL and the 2SC. For the 2SC phase with the chemical potential difference $\delta\mu = \mu_u - \mu_d$, this phenomena has been investigated in Ref.⁴⁵⁾. Recently, it has been suggested that the interior gap state may overcome the LOFF state if the coupling between heavy quark and light quark exceeds some critical coupling⁴⁶⁾. It would be interesting to study these other possibilities than the pure BCS state in our SD approach with the momentum-dependent improved coupling.

Acknowledgments

I am grateful to T. Hatsuda for fruitful discussions and suggestions during this work, and for reading of the manuscript. I wish to express my gratitude to T. Kunihiro for helpful advices on summarizing this paper at the last stage of the work. I would like to thank

A. Hayashigaki, S. Sasaki and K. Itakura for their useful comments and encouragements.

References

- 1) D.J. Gross and F. Wilczek, Phys. Rev. Lett. **30**, 1343 (1973).
- 2) H.D. Politzer, Phys. Rev. Lett. **30**, 1346 (1973).
- 3) J.C. Collins and M.J. Perry, Phys. Rev. Lett. **34**, 1353 (1975).
- 4) D. Bailin and A. Love, Phys. Rept. **107**, 325 (1984).
- 5) M. Alford, K. Rajagopal and F. Wilczek, Nucl. Phys. **B537**, 443 (1999).
- 6) For recent reviews, see :
K. Rajagopal and F. Wilczek, “*The Condensed Matter Physics of QCD*”, in “At the frontier of particle physics – handbook of QCD”, Volume 3, Chapter 35, edited by M. Shifman (World Scientific, 2001) [[hep-ph/0011333](#)];
M. G. Alford, Ann. Rev. Nucl. Part. Sci. **51** (2001) 131 [[hep-ph/0102047](#)];
T. Schafer, [hep-ph/0304281](#).
- 7) D.H. Rischke, [nucl-th/0305030](#).
- 8) N. Evans, J. Hormuzdiar, S.D.H. Hsu and M. Schwetz, Nucl. Phys. **B581**, 391 (2000).
- 9) D.K. Hong, Nucl. Phys. **B582**, 451 (2000).
- 10) T. Schäfer and F. Wilczek, Phys. Rev. **D60**, 074014 (1999).
- 11) M. Alford, J. Berges and K. Rajagopal, Nucl. Phys. **B558**, 219 (1999).
- 12) M. Buballa and M. Oertel, Nucl. Phys. **A703**, 770-784 (2002).
- 13) T. Schäfer, Nucl. Phys. **B575**, 269 (2000).
- 14) H. Abuki, T. Hatsuda and K. Itakura, Phys. Rev. **D65**, 074014 (2002).
- 15) W.E. Brown, J.T. Liu, and H.C. Ren, Phys. Rev. **D61**, 114012 (2000);
ibid. **D62**, 054013 (2000); *ibid.* **D62**, 054016 (2000).
- 16) P.W. Anderson and P. Morel, Physica **26**, 671 (1960);
P.W. Anderson and P. Morel, Phys. Rev. **123**, 1911 (1961).
- 17) R. Balian and N.R. Werthaner, Phys. Rev. **131**, 1553 (1963).
- 18) M. Iwasaki and T. Iwado, Phys. Lett. **B 350**, 163 (1995);
Prog.Theor.Phys.**94**, 1073 (1995).
- 19) M. Matsuzaki, Phys. Rev. **D62**, 017501 (2000).
- 20) S. Takagi, Prog. Theor. Phys. **109**, 233 (2003);
see also, M. Harada and S. Takagi, Prog. Theor. Phys. **107**, 561 (2002).
- 21) K. Higashijima, Phys. Rev. **D29**, 1228 (1984); Prog. Theor. Phys. Suppl. **104**, 1 (1991);

- V.A. Miransky, Sov. J. Nucl. Phys. **38**, 280 (1983);
P. Castorina, S-Y. Pi, Phys. Rev. **D31**, 411 (1985).
- 22) K-I. Aoki, T. Kugo and M. Mitchard, Phys. Lett. **B266**, 467 (1991). K-I. Aoki, M. Bando, T. Kugo and M. Mitchard, Prog. Theor. Phys. **84**, 683 (1990).
 - 23) R.D. Pisarski and D.H. Rischke, Phys. Rev. **D60**, 094013 (1999).
 - 24) R.D. Pisarski and D.H. Rischke, Phys. Rev. **D61**, 074017 (2000).
 - 25) T. Schäfer and F. Wilczek, Phys. Rev. **D60**, 114033 (1999).
 - 26) D.K. Hong, V.A. Miransky, I.A. Shovkovy and L.C.R. Wijewardhana, Phys. Rev. **D61**, 056001 (2000), Erratum-ibid.**D62**, 059903 (2000).
 - 27) R. Rapp, T. Schäfer, E.V. Shuryak, and M. Velkovsky, Phys. Rev. Lett.**81**, 53 (1998).
 - 28) M. Alford, K. Rajagopal, and F. Wilczek, Phys. Lett. **B422**, 247 (1998).
 - 29) T. Schäfer and F. Wilczek, Phys. Lett. **B450**, 325 (1999).
 - 30) K. Iida and G. Baym, Phys. Rev. **D63**, 074018 (2001).
 - 31) J.M. Cornwall, R. Jackiw and E. Tomboulis, Phys. Rev. **D10**, 2428 (1974).
 - 32) D. T. Son, Phys. Rev. **D 59**, 094019 (1999).
 - 33) J. Berges and K. Rajagopal, Nucl. Phys. **B538**, 215 (1999).
 - 34) G.W. Carter and D. Diakonov, Phys. Rev. **D60**, 016004 (1999).
 - 35) T.M. Schwarz, S.P. Klevansky and G. Papp, Phys. Rev. **C60**, 055205, (1999).
 - 36) M. Kitazawa, T. Koide, T. Kunihiro and Y. Nemoto, Prog. Theor. Phys. **108**, 929, (2002).
 - 37) T. Holstein, R.E. Norton and P. Pincus, Phys. Rev. **B6**, 2649 (1973);
M.Yu. Reizer, Phys. Rev. **B40**, 11571 (1988);
M.Yu. Reizer, Phys. Rev. **B44**, 5476 (1991).
 - 38) H. Abuki, (work in progress).
 - 39) M. Alford and K. Rajagopal, JHEP **0206** (2002) 031 [hep-ph/0204001].
 - 40) A.W. Steiner, S. Reddy and M. Prakash, Phys. Rev. D **66**, 094007 (2002) [hep-ph/0205201].
 - 41) I. Shovkovy and Mei Huang, Phys. Lett. **B564**, 205, (2003).
 - 42) A. Mishra and H. Mishra, hep-ph/0306105.
 - 43) A.I. Larkin and Yu.N. Ovchinnikov, Ah. Eksp. Teor. Fiz.**47**, 1136 (1964),
(Sov. Phys. JETP **20**,762 (1965)).
 - 44) P. Fulde and R.A. Ferrell, Phys. Rev. **135**, A550 (1964).
 - 45) M.G. Alford, J.A. Bowers and K. Rajagopal, Phys. Rev. **D63**, 074016 (2001).
 - 46) E. Gubankova, W. Vincent Liu and F. Wilczek, hep-ph/0304016.